Removal of Clutter and Random Noise for GPR Images

Buddepu Santhosh Kumar, *Student Member, IEEE*, Ajit Kumar Sahoo, *Member, IEEE*, and Subrata Maiti, *Member, IEEE*
Department of Electronics and Communication Engineering
National Institute of Technology, Rourkela Odisha, India
519ec1005@nitrkl.ac.in, ajitsahoo@nitrkl.ac.in, and smaiti@nitrkl.ac.in

***Abstract*—Ground Penetrating Radar (GPR) is one of the most efficient non-invasive geophysical methods for detecting subsurface anomalies, with many applications including landmine, cable, and pipe detection. GPR has the advantage of being able to detect both metallic and nonmetallic buried objects. However, clutters and noise can make it difficult to detect shallowly buried explosive devices. These effects must be removed to extract the target signature successfully. This article employs gradient magnitude with thresholding along with wavelet-based denoising for this purpose. Although gradient with thresholding-based techniques can effectively eliminate clutters such as antenna crosstalk and ground bounce, they cannot completely eliminate random noise. The random noise effects are then removed using wavelet-based denoising. To test the implemented methods, experimental GPR data collected in a facilitated laboratory environment and an accurate dataset offered by the electromagnetic software simulation tool gprMax are used. The results show that the proposed method outperforms traditional methods like mean removal and singular value decomposition (SVD) techniques in terms of peak signal to noise ratio (PSNR) and image entropy.**

***Index Terms*—GPR, gradient, mean removal, SVD, wavelet.**

I. Introduction

GPR is a geophysical technique that employs electro-magnetic (EM) waves to locate and image objects buried beneath the ground [1]. It is a non-invasive and non-destructive geophysical method that can be used to detect landmines, cables, pipes, reinforcement bars, fractures in the bedrock and the position of subsurface cavities, and also sediment and moisture. GPR is remarkably responsive to changes in a medium's EM characteristics, which allow both metallic and non-metallic objects to be detected [2]. GPR systems have a high detection probability and also have a high rate of false alarms. As a result, detecting buried objects efficiently and reliably is a challenging task. Several phenomena, including a transmitter to receiver antenna crosstalk, ground bounce, scattering from some of the other substances inside the soil surface (rocks, roots, pebbles, etc), noise caused by imperfections in the hardware, non-uniform geological structures, and so on, make detecting a subsurface object a difficult problem and cause clutter [3]. To reduce the false alarm rates, it's necessary to successfully extract target signals from clutters in GPR data analysis. Various clutter mitigation techniques are described in the literature for this purpose.

Average removal, which involves finding the mean of the received A-scans to obtain an estimate of the average signal trace, can remove the majority of the homogeneous ground bounce but fails to eliminate clutters in soils with high moisture and random noise [1]. Time gating based on entropy is a useful technique [4]. However, choosing a time window that covers clutters without hampering target response remains a challenge. Potin et al. [5] proposed a digital filter with optimized coefficients, but its limitation is the optimal selection of coefficients. maximum likelihood estimation (MLE) employs a hypothesis test to determine a threshold for removing ground bounce; however, it requires some prior knowledge of targets, and yields poor results for plastic targets [6], [7]. Wavelets provide better denoising results, but they cannot eliminate ground bounce as this requires some preprocessing [8]. Clutter reduction has been achieved using subspace-based statistical signal processing techniques like SVD [9]–[11], principal component analysis (PCA) [11]–[13], independent component analysis (ICA) [13], [14], and non-negative matrix factorization (NMF) [15], [16]. In SVD and PCA, the ground bounce is assumed to be spanned by the first dominant singular value or principal component, which is invalid if the surface is rough and heterogeneous. Furthermore, SVD removed the lower intensity part of the data, which is not cluttered but was treated as clutter by SVD in no target case. ICA depends on the statistical independence of components but practical GPR data is statistically dependent. NMF has a similar appearance to remaining subspace-based matrix decomposition algorithms, which differs from them by the fact that all of the decomposed matrices elements are non-negative. However, one significant disadvantage is that it ignores the geometric structure of the data and the main limitation of these subspace-based approaches is estimating the number of components which span target and clutter subspaces. PCA with Fuzzy C-Means (FCM) clustering has been proposed to resolve the manual selection of the number of subspace components [17]. PCA has been used to decompose the image into the target, clutter, and noise subspaces, and FCM has assigned the weights to each subspace based on its membership values. The newly proposed morphological component analysis (MCA) [18] decomposes target and clutters into the morphological components, each of which is sparsely depicted which uses suitable dictionaries.

978-1-6654-4175-9/21/$31.00

In this paper, gradient magnitude with Otsu's threshold is applied to the reconstructed image obtained from the PCA algorithm for the removal of clutters and random noise. However, it fails to remove the random noise completely. The wavelet based denoising is applied to the thresholded image. The implemented methods were tested on synthetic and experimental B-scan images, resulting in better PSNR and image entropy than that of mean removal and SVD techniques.

The remainder of the manuscript is structured as follows. Section II goes over how to implement the proposed method, which includes both gradient with thresholding and wavelet-based denoising for clutter and noise removal. Section III compares the proposed to state-of-the-art methods and deals with results for both synthetic and measured data. The paper comes to a close with Section IV, which outlines future research directions.

II. Proposed Method

A. Gradient-based clutter suppression

A directional change in the intensity of an image is known as an image gradient. At each image point, the gradient of a two-variable intensity function is a 2D vector with components determined by the derivatives in the horizontal and vertical directions. The gradient-based clutter suppression procedure is as follows:

1) Apply the PCA algorithm to a raw B-scan image to obtain the reconstructed B-scan image: The raw B-scan image be given as follows:

$$\mathbf{X}_{M\times N} = \begin{bmatrix} x_1 & x_2 & \cdots & x_N \end{bmatrix}_{M\times N}, \tag{1}$$

where M is the number of samples and N is the number of A-scans or offsets. The principal components in PCA can be calculated using the eigenvectors of the covariance matrix $\mathbf{C}$. The covariance matrix $\mathbf{C}$ is given by

$$\mathbf{C} = \frac{1}{N}\mathbf{X}\mathbf{X}^T. \tag{2}$$

Using Eigen decomposition, the eigenvalues and eigenvectors are computed using the following relation

$$\mathbf{C}\boldsymbol{\theta} = \boldsymbol{\theta}\boldsymbol{\Lambda}, \tag{3}$$

where $\boldsymbol{\theta}$ and $\boldsymbol{\Lambda}$ are respectively the eigenvectors and eigenvalues of $\mathbf{C}$. The first principal component consists of maximum energy which corresponds to reflections from the ground surface, not the target signal. The energy of some reflections from soil inhomogeneities and noise, on the other hand, corresponds to the last few principal components. To extract as much of the target signal as possible, consider forty-five percent of the principal components from the second as a better choice (based on several experiments), and the remaining components are discarded. The reconstructed B-scan data is given by the following:

$$\mathbf{X}_{rec} = \mathbf{X}\begin{bmatrix}\theta_2 & \theta_3 & \cdots & \theta_k\end{bmatrix}\begin{bmatrix}\theta_2 & \theta_3 & \cdots & \theta_k\end{bmatrix}^T, \tag{4}$$

where $\mathbf{X}_{rec}$ is reconstructed B-scan data, k is 45% of the total number of principal components. The reconstructed data from the PCA algorithm still consists of some echoes from soil in-homogeneities and other clutters; therefore, the gradient magnitude with thresholding-based clutter removal algorithm is used.

2) Calculate the gradient magnitude of the reconstructed B-scan using the Sobel kernel: A gradient is a measure of change in an image function in terms of how pixel values change in the horizontal or vertical directions. It is defined mathematically as

$$\nabla\mathbf{X}_{rec}(x,y) = \begin{bmatrix} G_x \\ G_y \end{bmatrix}, \tag{5}$$

where G_x and G_y are derivatives (gradients) in x and y directions respectively, and thus are described as follows:

$$G_x = \frac{\partial \mathbf{X}_{rec}(x,y)}{\partial x}, G_y = \frac{\partial \mathbf{X}_{rec}(x,y)}{\partial y}. \tag{6}$$

The gradient vector has two main characteristics: (a) it points in the direction of a most rapid increase in intensity, and (b) the magnitude is the gradient direction's highest rate of increase. The gradient magnitude X_M is given as

$$X_M = |\mathbf{X}_{rec}(x,y)| = \sqrt{G_x^2 + G_y^2}. \tag{7}$$

Finite differences provide a numerical solution to differential equations using an approximation of derivatives. In this work, the Sobel kernel was applied to a reconstructed image in a cross-correlation framework to generate gradients in the $x-$ and $y-$ directions [19]. Sobel filters are better enough to eliminate gaussian noise, whereas laplacian of gradient (LOG) or bilateral filters are used to remove impulse noise. The Sobel kernels are depicted in the figure below.

-1	-2	-1
0	0	0
1	2	1

(a)

-1	0	1
-2	0	2
-1	0	1

(b)

Fig. 1: Sobel kernels (a) $x-$direction kernel (b) $y-$direction kernel

3) Calculate the intensity threshold using Otsu's algorithm, and remove the B-scan data that doesn't satisfy the thresholding criterion: Otsu's method is an algorithm that determines the intensity threshold which optimally divides data into two categories: foreground and background. It is accomplished by optimizing a measure called between-class variance [20]. This variance is given as follows:

$$\sigma_B^2 = W_b W_f(\mu_b - \mu_f)^2, \tag{8}$$

where W_b and W_f are the ratios of background and foreground pixels to total pixels, and μ_b and μ_f are the average intensity of background and foreground. If our image has Intensity homogeneities, it means there is no local variation in both the background and the foreground. We can use global thresholding if there isn't any local variation. If we want to use global

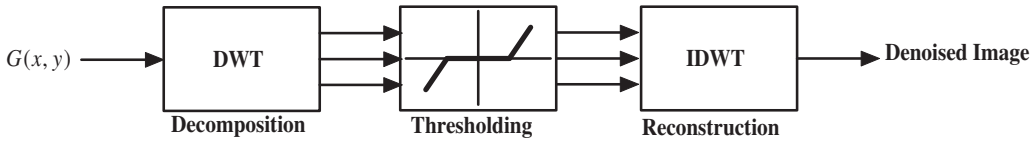

Fig. 2: Wavelet based Denoising process.

thresholding and the foreground and background are clearly distinct, otsu's method is appropriate. It is a standard method and usually gives satisfying results. It initially computes the intensity histogram for the image. Otsu's algorithm will select all possible values for the intensity threshold and calculate the between-class variance. The optimal threshold intensity is the intensity that produces the highest variance. This can be done using the following:

$$G(x,y) = \begin{cases} \mathbf{X}_{rec}(x,y), & X_M \geq threshold \\ 0, & others \end{cases} \tag{9}$$

where $G(x,y)$ is data after gradient-based clutter removal. As the gradient-based algorithm will not be able to remove all the clutters, particularly random noise, wavelet-based denoising will be used to reduce clutters and noise.

B. Wavelet-based De-noising

A wavelet is a short-duration waveform with an average value of zero that provides both time and frequency information at the same time. As illustrated in Fig. 2, the wavelet denoising [21] process consists primarily of three steps. (a) wavelet analysis (decomposition), (b) thresholding and denoising, and (c) synthesis (reconstruction). In the wavelet decomposition step, the desired wavelet and level are selected. After numerous trials, the Daubechies 7 (db7) wavelet with the 7th level has been used in this paper for better denoising results. The signal is decomposed into approximation and detailed coefficients. Detailed coefficients are thresholded in this analysis because the detailed coefficients capture abrupt changes in the signal and must be preserved after noise removal. In the thresholding and denoising step, noise removal is accomplished by nullifying the coefficients that are less than the threshold. The threshold is calculated using the square root log method and is given by [22]

$$T_j = \sigma_j \sqrt{N_j} \tag{10}$$

$$\sigma_j = \frac{median(|w_c|)}{0.6745}, \tag{11}$$

where σ_j is the median absolute deviation, N_j is the noisy signal length at jth decomposition level and w_c is wavelet coefficient at decomposition level j. In the wavelet reconstruction step, use the inverse process of decomposition with approximation coefficients and modified detailed coefficients. In terms of denoising, the signal coefficients for reconstruction remain constant. However, for image decomposition (with dwt and idwt), it will be half the size of the original signal. The reconstruction quality is determined by the norms and histogram; the smaller the norms, the closer the value (say L2). If the number of coefficients and dimensions do not match, MATLAB will not allow reconstructing; instead, zero padding will be performed. The flowchart in Fig. 3 depicts the proposed clutter and noise removal process.

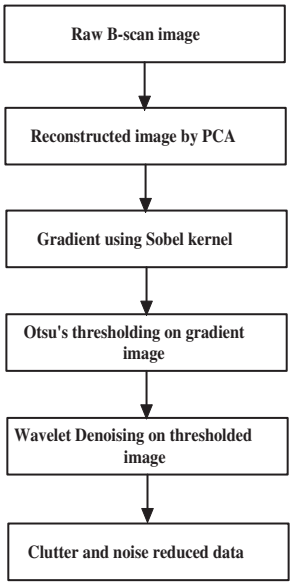

Fig. 3: Flow chart of the proposed technique.

III. Experimental Results and Analysis

In this paper, the proposed and the state-of-the-art techniques are applied to synthetic as well as real GPR data. All the experiments are carried out on the R2019b MATLAB, with an Intel(R) Core(TM) i5-7500 CPU 3.40GHz, 4 GB RAM and 64-bit operating system. These techniques are quantified using PSNR and image entropy.

$$PSNR\ (dB) = 10\log_{10}\frac{L^2}{MSE}, \tag{12}$$

where $L = 255$ for an $8-$bit image or $L = 1$ for a normalized image, and *MSE* is the mean square error, which is a metric of image quality.

$$MSE = \frac{1}{MN}\sum_{m=0}^{M-1}\sum_{n=0}^{N-1}\left(X_{mn} - Y_{mn}\right)^2, \tag{13}$$

where X_{mn} is calculated by subtracting the target-free GPR image from the target-containing GPR image. It only includes information that is relevant to the target and Y_{mn} is a reduced cluttered image. The image entropy is given as

$$H = \frac{\left(\sum_{m=0}^{M-1}\sum_{n=0}^{N-1} B^2(m,n)\right)^2}{\left(\sum_{m=0}^{M-1}\sum_{n=0}^{N-1} B^4(m,n)\right)}. \tag{14}$$

A higher PSNR indicates better image reconstruction quality, while lower image entropy indicates improved clutter rejection performance.

A. *Synthetic Data Results*

gprMax is a Finite Difference Time Domain (FDTD) based simulation software for simulating different types of GPR scenarios. In this paper, we tested the proposed technique on various targets such as metal pipe, metal sheet, plastic pipe, metal cylinder, and plastic cylinders. One of the simulation configurations is depicted in Fig. 4.

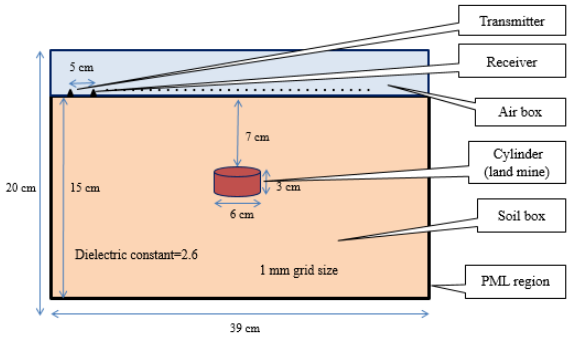

Fig. 4: The experimental scenario of simulation data.

The dimensions of the box (domain) are $39 \times 10 \times 20$ cm, and it is filled with sand up to 15cm, with a dielectric constant of 2.6 and an air gap of 5cm. The antenna moves along the scan-axis in steps of 1 cm from 0 to 39 cm. The pulse that is transmitted is a Gaussian signal with a center frequency of 2 GHz, a time window chosen as 5 ns. A PEC metal cylinder with dimensions of 3 cm height and 6 cm diameter is buried 7 cm below the soil surface as the buried target. A total of 32 A-scans are generated, which are then concatenated to form the raw B-scan. Gradient clutter suppression along with wavelet denoising technique and state-of-the-art techniques are applied on simulated data and the results are shown in the figure below. An image of raw B-scan data is shown in Fig. 5 (a), the target's hyperbolic signature has receded due to static clutter. In practice, Gaussian noise describes a variety of clutters. To replicate real-world scenarios, Gaussian noise of 5 dB, 15 dB, and 30 dB is added to the raw image. Fig. 5 (b) shows the SNR of 15 dB added to the raw image. The reconstructed image after the PCA algorithm successfully eliminates ground bounce (static clutter as shown in Fig. 5 (b)) but partially eliminates random noise. Gradient-based thresholding is applied to the reconstructed image. The obtained threshold from Otsu's method is 0.0395. It is removing a significant amount of clutter and random noise, but it is still unable to completely remove random noise as shown in Figs. 5 (c) and (d). Further, wavelet-based denoising removes the majority of the random noise as depicted in Fig. 5 (e). The proposed algorithm provides better PSNR and image entropy when compared to state-of-the-art techniques. Table I shows the image entropy and PSNR values for the aforementioned techniques.

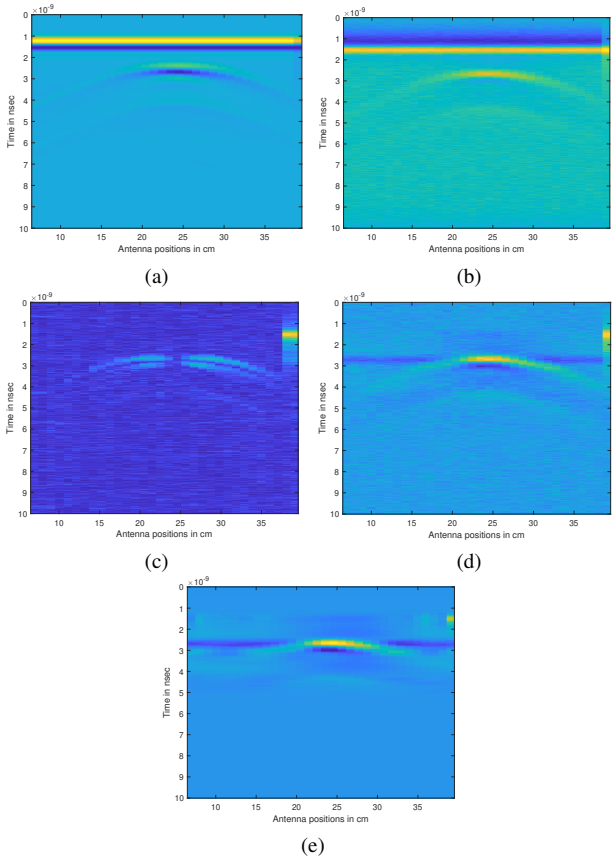

Fig. 5: Simulation Results for SNR=15 dB (a) original B-scan data, (b) noisy Image, (c) gradient magnitude image, (d) image after Otsu's threshold, and (e) wavelet denoised image.

B. *Measured Data Results*

A laboratory setup is being considered for real-time data acquisition. Figs. 6 and 7 depict the schematic and experimental setups respectively. The horn antenna is used for transmitting and receiving the data at frequencies ranging from 800 MHz to 4 GHz, and it is connected to the VNA via an RF cable.

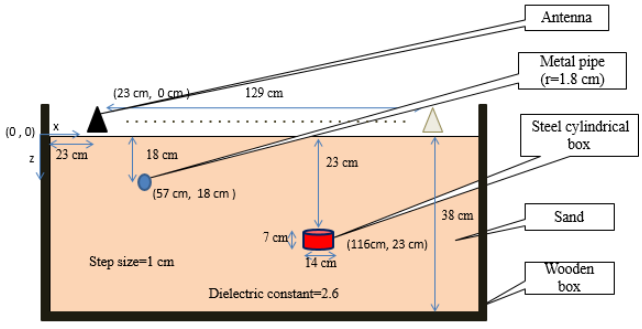

Fig. 6: Schematic of the setup.

The details of the experiment and model of laboratory setup are discussed below. The dimensions of the box (domain) are $155 \times 50 \times 41$ cm, and it is filled with sand up to 38 cm, with a dielectric constant of 2.6 and an air gap of 3 cm. The antenna moves along the scan-axis from 0-129 cm with a step size of

TABLE I: Image entropy and PSNR comparisons of simulation data.

Methods	Image entropy			PSNR (dB)		
	SNR=30 dB	SNR=15 dB	SNR=5 dB	SNR=30 dB	SNR=15 dB	SNR=5 dB
Raw data	5630.5	7850.1	21392	15.01	14.36	13.02
Mean removal	947.82	2421.9	11487	28.61	23.11	15.10
SVD	782.63	2218.8	11365	29.03	23.32	16.87
PCA	769.22	1621.5	9311.1	29.59	24.97	17.18
PCA with FCM	713.47	1425.1	8823.6	30.78	26.03	19.92
Propsed method	**647.54**	**1007.2**	**3661.2**	**34.73**	**31.69**	**25.96**

1 cm. Two targets, a metal pipe having a length of 57 cm and a radius of 1.8 cm and a steel box having a length of 7 cm and a radius of 7 cm, are buried inside the sand. The depth of the metal pipe is 18 cm and the steel box is 23 cm from the sand surface.

Fig. 7: Experimental setup in GPR lab.

A total of 130 A-scans are generated, which are then concatenated to form the raw B-scan. Gradient clutter suppression along with wavelet denoising technique and state-of-the-art techniques are applied on measured data and the results are shown in Fig. 8. The hyperbolic signatures of targets have faded due to antenna coupling and ground bounce, as shown in Fig. 8 (a). The reconstructed image after the PCA algorithm can partially eliminate random noise and soil in-homogeneities by ignoring the least significant principal components. Gradient-based thresholding is applied to the reconstructed image. The obtained threshold from Otsu's method is 0.0013. It is removing a significant amount of clutter and random noise, but it is still unable to completely remove some portions of clutter as shown in Figs. 8 (b) and (c). Further, wavelet-based denoising removes the majority of the random noise as depicted in Fig. 8 (d). The proposed algorithm provides better PSNR and image entropy when compared to state-of-the-art techniques. Table II shows the image entropy and PSNR values for the aforementioned techniques.

TABLE II: Image entropy and PSNR comparisons of measured data.

Methods	Image entropy	PSNR (dB)
Raw data	6559.6	22.41
Mean removal	2859.2	31.69
SVD	2794.5	32.09
PCA	1915.9	33.24
PCA with FCM	1537.2	34.88
Proposed method	**698.37**	**37.28**

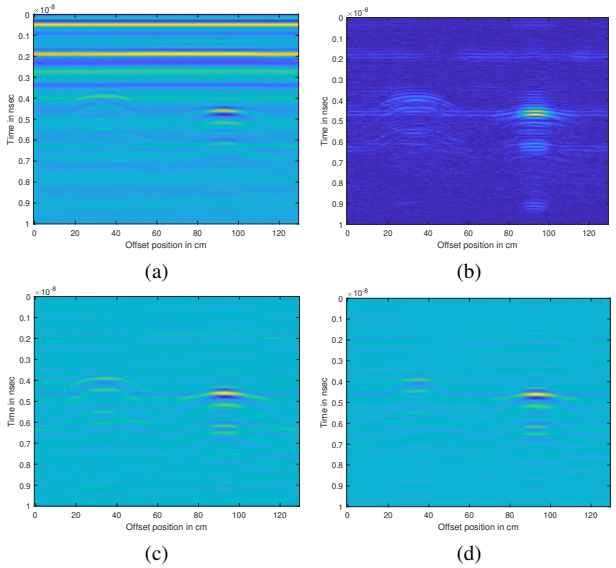

Fig. 8: Measured data Results (a) Original B-scan image, (b) Gradient magnitude image, (c) Image after Otsu's threshold, and (d) Wavelet denoised image.

IV. Conclusion and Future Work

This paper proposed clutter and noise removal using gradient magnitude with thresholding along with wavelet-based denoising. While gradient with thresholding-based techniques can effectively eliminate clutters like antenna crosstalk and ground bounce, they can't completely eliminate random noise. Wavelet-based denoising is then used to remove the random noise effects. The proposed method outperforms state-of-the-art methods in terms of clutter suppression, PSNR, and entropy, according to simulated and measured data results. However, the proposed method has been validated in homogeneous medium, and the efficacy of the implemented techniques will need to be validated in a highly cluttered environment with heterogeneous soils, rough surfaces, and various fields with varying moisture levels in future research.

V. Acknowledgment

This research was supported by the IMPRINT II project on the Development of Ground Penetrating Radar for Detection of Subsurface Objects sponsored by SERB, INDIA.

References

[1] D. J. Daniels, *Ground penetrating radar*, vol. 1. IET, 2004.
[2] F. Abujarad, "Ground penetrating radar signal processing for landmine detection," 2007.

[3] A. M. B. da Costa, D. Martins, D. Rodrigues, L. Fernandes, R. Moura, and Áurea Madureira-Carvalho, "Ground penetrating radar for buried explosive devices detection: A case studies review," *Australian Journal of Forensic Sciences*, vol. 0, no. 0, pp. 1–20, 2021.

[4] R. Solimene, A. Cuccaro, A. Dell'Aversano, I. Catapano, and F. Soldovieri, "Ground clutter removal in gpr surveys," *IEEE Journal of Selected Topics in Applied Earth Observations and Remote Sensing*, vol. 7, no. 3, pp. 792–798, 2014.

[5] D. Potin, E. Duflos, and P. Vanheeghe, "Landmines ground-penetrating radar signal enhancement by digital filtering," *IEEE Transactions on Geoscience and Remote Sensing*, vol. 44, no. 9, pp. 2393–2406, 2006.

[6] K. Ho and P. Gader, "A linear prediction land mine detection algorithm for hand held ground penetrating radar," *IEEE Transactions on Geoscience and Remote Sensing*, vol. 40, no. 6, pp. 1374–1384, 2002.

[7] F. Abujarad, A. Jostingmeier, and A. Omar, "Clutter removal for landmine using different signal processing techniques," in *Proceedings of the Tenth International Conference on Grounds Penetrating Radar, 2004. GPR 2004.*, pp. 697–700, 2004.

[8] F. Abujarad, G. Nadim, and A. Omar, "Wavelet packets for gpr detection of non-metallic anti-personnel land mines based on higher-order-statistic," in *Proceedings of the 3rd International Workshop on Advanced Ground Penetrating Radar, 2005. IWAGPR 2005.*, pp. 21–25, 2005.

[9] B. Cagnoli and T. Ulrych, "Singular value decomposition and wavy reflections in ground-penetrating radar images of base surge deposits," *Journal of Applied Geophysics*, vol. 48, no. 3, pp. 175–182, 2001.

[10] M. M. Riaz and A. Ghafoor, "Information theoretic criterion based clutter reduction for ground penetrating radar," *Progress In Electromagnetics Research B*, vol. 45, pp. 147–164, 2012.

[11] P. Sharma, B. Kumar, D. Singh, and S. Gaba, "Critical analysis of background subtraction techniques on real gpr data.," *Defence Science Journal*, vol. 67, no. 5, 2017.

[12] V. Kabourek, P. Černỳ, and M. Mazánek, "Clutter reduction based on principal component analysis technique for hidden objects detection.," *Radioengineering*, vol. 21, no. 1, 2012.

[13] B. Karlsen, J. Larsen, H. Sorensen, and K. Jakobsen, "Comparison of pca and ica based clutter reduction in gpr systems for anti-personal landmine detection," in *Proceedings of the 11th IEEE Signal Processing Workshop on Statistical Signal Processing (Cat. No.01TH8563)*, pp. 146–149, 2001.

[14] A. Zhao, Y. Jiang, W. Wang, and X. Jiaotong, "Exploring independent component analysis for gpr signal processing," in *Progress In Electromagnetics Research Symposium*, pp. 750–753, 2005.

[15] D. Kumlu and I. Erer, "Clutter removal in gpr images using non-negative matrix factorization," *Journal of Electromagnetic Waves and Applications*, vol. 32, no. 16, pp. 2055–2066, 2018.

[16] Y.-X. Wang and Y.-J. Zhang, "Nonnegative matrix factorization: A comprehensive review," *IEEE Transactions on Knowledge and Data Engineering*, vol. 25, no. 6, pp. 1336–1353, 2013.

[17] M. M. Riaz, A. Ghafoor, and V. Sreeram, "Fuzzy c-means and principal component analysis based gpr image enhancement," in *2013 IEEE Radar Conference (RadarCon13)*, pp. 1–4, 2013.

[18] E. Temlioglu and I. Erer, "Clutter removal in ground-penetrating radar images using morphological component analysis," *IEEE Geoscience and Remote Sensing Letters*, vol. 13, no. 12, pp. 1802–1806, 2016.

[19] N. Kanopoulos, N. Vasanthavada, and R. Baker, "Design of an image edge detection filter using the sobel operator," *IEEE Journal of Solid-State Circuits*, vol. 23, no. 2, pp. 358–367, 1988.

[20] S. L. Bangare, A. Dubal, P. S. Bangare, and S. Patil, "Reviewing otsu's method for image thresholding," *International Journal of Applied Engineering Research*, vol. 10, no. 9, pp. 21777–21783, 2015.

[21] S. R. Thatiparthi, R. R. Gudheti, and V. Sourirajan, "Mst radar signal processing using wavelet-based denoising," *IEEE Geoscience and Remote Sensing Letters*, vol. 6, no. 4, pp. 752–756, 2009.

[22] J. Shi, B. Lv, Y. Li, Y. Jia, R. Wang, and Y. Liao, "A new wavelet thresholding method based on cyclostationarity for enhancing the interception of computer video leakage signals," in *2018 17th IEEE International Conference On Trust, Security And Privacy In Computing And Communications/ 12th IEEE International Conference On Big Data Science And Engineering (TrustCom/BigDataSE)*, pp. 1901–1906, 2018.